FULL LENGTH ARTICLE

Multi-omics integration reveals potential stage-specific druggable targets in T-cell acute lymphoblastic leukemia

Zijun Yan [a,b], Jie Xia [e], Ziyang Cao [a,b], Hongyang Zhang [a,b], Jinxia Wang [a,b], Tienan Feng [a,d], Yi Shu [c,**], Lin Zou [a,b,c,*]

[a] Clinical Research Unit, Shanghai Children's Hospital, School of Medicine, Shanghai Jiao Tong University, Shanghai 200062, China
[b] Institute of Pediatric Infection, Immunity, and Critical Care Medicine, Shanghai Jiao Tong University School of Medicine, Shanghai 200062, China
[c] Center for Clinical Molecular Laboratory Medicine of Children's Hospital of Chongqing Medical University, Chongqing 400014, China
[d] Clinical Research Institute, Shanghai Jiao Tong University School of Medicine, Shanghai 200025, China
[e] Bioinformatics and BioMedical Bigdata Mining Laboratory, School of Big Health, Guizhou Medical University, Guiyang, Guizhou 554300, China

Abstract   T-cell acute lymphoblastic leukemia (T-ALL), a heterogeneous hematological malignancy, is caused by the developmental arrest of normal T-cell progenitors. The development of targeted therapeutic regimens is impeded by poor knowledge of the stage-specific aberrances in this disease. In this study, we performed multi-omics integration analysis, which included mRNA expression, chromatin accessibility, and gene-dependency database analyses, to identify potential stage-specific druggable targets and repositioned drugs for this disease. This multi-omics integration helped identify 29 potential pathological genes for T-ALL. These genes exhibited tissue-specific expression profiles and were enriched in the cell cycle, hematopoietic stem cell differentiation, and the AMPK signaling pathway. Of these, four known druggable targets (CDK6, TUBA1A, TUBB, and TYMS) showed dysregulated and stage-specific expression in malignant T cells and may serve as stage-specific targets in T-ALL. The TUBA1A expression level was higher in the early T cell precursor (ETP)-ALL cells, while TUBB and TYMS were mainly highly expressed in malignant T cells arrested at the CD4 and CD8 double-positive or single-positive stage. CDK6 exhibited a U-shaped expression pattern in malignant T cells along the naïve

* Corresponding author. Clinical Research Unit, Shanghai Children's Hospital, School of Medicine, Shanghai Jiao Tong University, Shanghai 200062, China.
** Corresponding author.
E-mail addresses: shu_yi@hospital.cqmu.edu.cn (Y. Shu), zoulin@shchildren.com.cn (L. Zou).
Peer review under responsibility of Chongqing Medical University.

to maturation stages. Furthermore, mebendazole and gemcitabine, which target TUBA1A and TYMS, respectively, exerted stage-specific inhibitory effects on T-ALL cell lines, indicating their potential stage-specific antileukemic role in T-ALL. Collectively, our findings might aid in identifying potential stage-specific druggable targets and are promising for achieving more precise therapeutic strategies for T-ALL.

Introduction

T-cell acute lymphoblastic leukemia (T-ALL) is an aggressive hematologic tumor caused by the malignant transformation of a hematopoietic progenitor leading to the maturation arrest.[1] The treatment protocols of patients with T-ALL are based on risk stratification.[2] With conventional chemotherapy, approximately 20% of pediatric and 50% of adult T-ALL patients are unable to achieve a durable complete remission,[3,4] possibly caused by the inability of eradicating the whole leukemic cell population.

T-ALL is highly heterogeneous and is classified into groups characterized by unique gene expression signatures and immunophenotypic profiles that reflect thymocyte developmental arrest at different stages.[5,6] For example, T-ALL is divided into four immunophenotypes (namely, pre-, pro-, cortical-, and mature-T-ALL) in analogy to T cell maturation by the expression of the cell surface markers.[5] In addition, T-ALL patients arrested at the early T-cell precursor (ETP) stage have been identified as a distinct high-risk subgroup.[7] Liu et al classified T-ALL into eight molecular subtypes on the basis of ectopic expression of transcription factors (TFs): TAL1, TAL2, TLX1, TLX3, HOXA, LMO1/LMO2, LMO2/LYL1, and NKX2-1.[6] Intergroup heterogeneity poses formidable challenges in developing targeted and effective therapeutic regimens for T-ALL patients. Therefore, there is an urgent need to examine stage-specific aberrances in T-ALL, which might help develop targeted therapies for this disease.

Targeted therapies were developed for T-ALL on the basis of its molecular characterization.[8−12] For example, the identification of activating NOTCH1 mutations promoted much interest in exploring molecularly tailored therapies and initiation of clinical trials to block NOTCH1 signaling with gamma-secretase inhibitors.[8] Moreover, because of the effectiveness of ABL1 kinase inhibitors for the treatment of BCR-ABL1-positive T-ALL patients and the sensitivity of NUP214-ABL1 to these inhibitors,[9] NUP214-ABL1-positive T-ALL patients may benefit from the inclusion of ABL1 inhibitors in their treatment plans. Similarly, JAK/STAT inhibitors, currently under development for myeloproliferative disease treatment, might help treat T-ALLs by activating IL7R or JAK1 mutations.[10,12]

In past decades, one-dimensional omics analysis involving transcriptomic, epigenetic, or functional experiment technology has helped identify potential therapeutic targets for T-ALL.[13−15] For example, BRD4 was identified as an epigenetic target required for persisting cell survival in leukemia resistance.[13] A genome-wide clustered regularly interspaced short palindromic repeats (CRISPR) screen helped identify CDK6 as a potential therapeutic target for T-ALL.[14] Inhibition of the PI3Kγ and PI3Kδ isoforms is a candidate strategy for targeting PTEN-null T-ALL.[16] However, the one-dimensional omics approach often did not completely exploit the tumor genome and ignored T-ALL heterogeneity; in comparison, the multi-omics approach provides more comprehensive options for identifying molecular alterations and helps obtain more profound insights into disease pathogenesis.[17] Multi-omics data integration has also aided in drug repositioning, that is, new applications of approved or investigational drugs have been reasonably expanded.[18,19] The rapid developments in single-cell RNA sequencing (scRNA-seq) technology have enabled researchers to investigate the cell-type composition and to classify developmental lineages at the single-cell level.[20] Such research greatly advances our understanding of tumor cell heterogeneity.

In the current study, we performed multi-omics integration of transcriptome (including bulk tissue and single-cell), epigenome, and gene dependency database to identify potential stage-specific druggable targets and repositioned drugs for T-ALL. We hope that the information presented here will provide new insight into identifying potential stage-specific druggable targets and offer promise in achieving a more precise therapeutic strategy for T-ALL.

Materials and methods

Multi-omics data acquisition and processing

Public bulk transcriptomic datasets of T-ALL patients and normal controls were downloaded from Gene Expression Omnibus (GEO; www.ncbi.nlm.nih.gov/geo; GSE26713[21] and GSE48558[22]) and from a study by Erarslan-Uysal et al[23] (Table 1). We also downloaded bulk RNA-sequencing (RNA-seq) data and clinical information of 264 T-ALL patients from the Therapeutically Applicable Research to Generate Effective Treatments (TARGET) website (https://ocg.cancer.gov/programs/target/data-matrix).[6] Bulk RNA-seq data of 13 patients with T-ALL and four normal controls had been obtained from the Children's Hospital of Chongqing Medical University (CHCQMU) in our previous study.[24] scRNA-seq data of six patients with T-ALL were downloaded from Zenodo Biorepository (https://zenodo.org/record/

4756105#.YMbypC0RqqB).[25] scRNA-seq data for T-cell development from the normal developing human thymus (including 15 prenatal and nine postnatal thymic samples) were downloaded from Park et al (https://developmental.cellatlas.io/).[26] Epigenomic data for T-ALL were downloaded from the study by Erarslan-Uysal et al, which included assays for transposase-accessible chromatin using sequencing (ATAC-seq) data for 19 T-ALL patients and six normal thymus controls.[23]

Batch effects between independent transcriptomic datasets were corrected using the "ComBat" function of the "sva" R package. The "limma" R package was used to identify differentially expressed genes (DEGs) or differentially accessible peaks (DAPs) between tumor and normal control samples.[27] A DEG or DAP was identified if its adjusted p-value (adj$P$-value) was less than 0.05 and the absolute fold change (FC) value was larger than 1. According to Erarslan-Uysal et al, peaks were annotated by the nearest genes.[23]

Using the keyword "Acute Lymphoblastic Leukemia (ALL), T-cell" to search the cancer dependency map (DepMap) portal (data version: 22Q1; https://depmap.org/portal/download/all/),[28] the effect scores about five human T-ALL cell lines (SUP-T1, JURKAT, KE-37, PF-382, HSB2) were obtained. Genes with negative effect scores for all five T-ALL cell lines were considered potential dependency genes for T-ALL.

Interaction network and functional enrichment analysis

Protein−protein interaction (PPI) enrichment of the PPGs was analyzed using multiple protein modules of the STRING server (https://string-db.org/).[29] Gene−gene interactions (GGIs) of PPGs were evaluated using the GeneMANIA web tool (http://genemania.org).[30]

Enrichment analyses, including biological process (BP) and Kyoto Encyclopedia of Genes and Genomes (KEGG) pathways of PPGs, were conducted using the "enrichGO" and "enrichKEGG" functions of the "clusterProfiler"[31] R package. The enriched terms were filtered, with the p-value being adjusted using the Benjamini-Hochberg method (adj. P-value <0.05). Tissue enrichment results were downloaded from the STRING server.

Functional association test

The functional association test was performed as reported by Ni et al.[32] We speculated that, if our PPGs were functionally associated with known T-ALL-associated genes, then they would be close to each other in the functional association network, that is, they would have a significantly lesser shortest-path length in the network than random genes would.

Known T-ALL-associated genes were downloaded from the genetic association database (GAD) (http://geneticassociationdb.nih.gov).[33] The shortest path lengths between each pair of genes in the functional association network database, FunCoup, were measured using Dijkstra's algorithm.[34] The mean distance for PPGs was measured as the distance between the PPGs identified in our study and T-ALL-associated genes. Next, the same number of genes and PPGs was selected, and the above-mentioned procedures were repeated 1000 times. The P-value was calculated on the basis of the probability that the distance for the randomly selected genes was lesser than or equal to that for the PPGs. A P-value of less than 0.05 was considered statistically significant.

Drug−target network construction and drug sensitivity analysis

Data pertaining to candidate gene-targeting drugs, indications, targeted pathways, and associated conditions were obtained from the DrugBank database (https://go.drugbank.com/).[35] The network was visualized using the Cytoscape software (https://cytoscape.org/, version 3.8.2).

RNA-seq gene expression data of cancer cell lines were downloaded from Cancer Cell Line Encyclopedia (CCLE) (https://sites.broadinstitute.org/ccle/datasets).[36] The sensitivity scores (z-score) of candidate drugs against T-ALL cell lines were downloaded from The US National Cancer Institute 60 human cancer cell lines (NCI-60) database, which can be accessed via CellMiner (http://discover.nci.nih.gov/cellminer).[37] A z-score larger than 0 for a drug represented cell line sensitivity for the respective drug.

Molecular docking analysis

3D protein structures were downloaded from the PDB website (https://www.rcsb.org).[38] Discovery Studio v18[39] was used to remove water and unnecessary ligands of proteins. The 2D or 3D structures of drugs were downloaded from the ZINC (https://zinc.docking.org/)[40] and PubChem (https://pubchem.ncbi.nlm.nih.gov/) websites.[41] PyMOL (www.pymol.org) was used to convert 2D structures to 3D structures. The 2D or 3D structures of six drugs, that is, DB03461, DB14009, DB00707, DB06042, DB03800, and DB01643, were not found. The AutoDock Vina[42] wizard was used to perform molecular docking to obtain different conformations and corresponding binding energy scores (ESs). A binding ES of less than −5.0 kcal/mol was considered to indicate potential stable binding affinity.[43]

scRNA-seq data analysis

scRNA-seq data analysis was performed using the "Seurat" R package (version 4.0).[44] Genes with a scaled expression value larger than 0 and expressed in at least 35% of malignant T-cells were considered highly expressed genes. The "RunUMAP" function was used to embed the cells in a two-dimensional map.

Developmental trajectory analysis was performed using the "Monocle" R package (version 2.1.6; http://cole-trapnell-lab.github.io/monocle-release/).[45] Genes differentially expressed across different cell types were identified with the "differentialGeneTest" function, and the DDRTree dimensionality reduction method was used to construct the pseudotime trajectory. Each cell was assigned a pseudotime value based on its position along the trajectory.

Cell culture

T-ALL cell lines PEER (DSMZ, #ACC6) and P12 (DSMZ, #ACC34) were purchased from the vendors. MOLT3, MOLT4, CUTTL1, CCRF-CEM, and JURKAT were thawed from our stock (Ref. 24). All the T-ALL cell lines were cultured in RPMI-1640 (Invitrogen, USA) supplemented with 10% fetal bovine serum (Invitrogen, USA), L-glutamine and penicillin/streptomycin (Invitrogen, USA).

Flow cytometry assay

A total of 5×10^5 T-ALL cells were rinsed twice with phosphate buffer solution (PBS). Next, the nonspecific IgG binding sites on the cell were blocked with the Human Fc Block Reagent (BD Biosciences, 564,219) at 4 °C for 30 min. After blocking, the cells were aliquoted into tubes and stained with the antibody cocktails at 4 °C in the dark room for 30 min. Subsequently, the cells were rinsed again with cold PBS, and then collected after centrifugation (300 g/min, 5 min). The surface markers of cells were detected by flow cytometry (BD FACSAria™ II). The results were analyzed by BD FACSDiva software (Version 8.0.2). The antibodies used in the research were listed: anti-CD3 (BD Biosciences, 557,832), anti-CD2 (BD Biosciences, 562,638), anti-CD5 (BD Biosciences, 340,583), anti-CD1a (BD Biosciences, 559,775), anti-CD34 (BD Biosciences, 652,802), anti-CD4 (BD Biosciences, 557,852), anti-CD8 (BD Biosciences, 555,367), and anti-CD45 (Invitrogen, 11-9459-42) antibodies.

Western blotting

Cells were rinsed with the phosphatase-inhibitor cocktail (Roche, Cat#: B15001) containing cold PBS buffer twice, and then lysed in RIPA buffer containing phosphatase-inhibitor cocktail and a mixture of protease inhibitors (Cømplete, Roche). The cell debris was removed by centrifuging the lysates at 13,000 g. After denaturing the protein by incubating at 95 °C within Laemmli sample buffer for 5 min, the total protein was run on 6%–12% PAGE gels and transferred onto polyvinylidene difluoride (PVDF) membranes. Membranes were blocked using TBS-T and bovine serum albumin (BSA) and then probed with primary antibodies overnight at 4 °C. The following day blots were rinsed and incubated with horseradish peroxidase (HRP)-conjugated secondary antibodies. Blots were detected using the chemiluminescent substrate and SynGene imaging system. Quantitative analysis was performed using Photoshop software. The antibodies used in the research were listed: GAPDH (Proteintech, HRP-60004), PLCγ1 pY783 (Cell Signaling, 14,008), ZAP-70 pY319 (Cell Signaling, 2701).

Cell counting kit-8 (CCK8) assay

About 2×10^4 human T-ALL cells (PEER, MOTL3, MOLT4, CUTTL1, P12, CCRF-CEM, and JURKAT) treated with different concentrations of the drug were suspended and plated in a 96-well plate (100 μL/well), and pre-incubated in a humidified incubator containing 5% CO_2 at 37 °C for 48 h. Subsequently, 10 μL of the CCK-8 solution (Dojindo, Japan) was added to each well of the plate, followed by incubation at 37 °C for 3 h. The absorbance at 450 nm was measured using an enzyme immunoassay analyzer (Bio-Tek, Winooski, VT, USA).

Statistical analysis

Statistical analysis was mainly performed using the R software (version 4.0.0, https://www.r-project.org/). The Venn plot was visualized using the "venn.diagram" function in the "VennDiagram" R package. Principal component analysis (PCA) was performed using the "prcomp" function and visualized using the "factoextra" R package. Using the "cor.test" function, the correlation between PPG expression and accessibility was calculated with the Spearman correlation coefficient, and the expression correlation of PPGs was calculated with the Pearson correlation coefficient. The Wilcoxon test was used to test whether any of the differences between two groups were statistically significant. The Kruskal–Wallis test was applied to compare differences across multiple groups, for example, for white blood cell counts (WBCs). Hierarchical clustering was performed with "hclust" functions and visualized using the "pheatmap" R package. Event-free survival (EFS) and overall survival (OS) were used to assess the association between PPG expression and prognosis. The log-rank test and Kaplan–Meier (KM) curve were used for survival analysis. The survival curve was plotted using the "Survival" and "SurvMiner" R packages.

Results

Multi-omics integration–based identification of PPGs of T-ALL

To systemically analyze the molecular changes in and identify potential stage-specific therapeutic targets for T-ALL, we used a multi-omics integration approach, including transcriptomic-, epigenomic-, and gene-dependency database–based analyses (Fig. 1). For transcriptomic analysis, we compared the gene expression profiles between T-ALL patients and normal controls from three independent cohorts (Table 1).[21–23] We selected 108 DEGs whose expression levels were up-regulated in T-ALL patients in all three cohorts (Fig. 2A). For epigenomic analysis, we compared chromatin accessibility between T-ALL patients and normal thymus controls and identified a total of 15,306 opened DAPs (Fig. 2B; Fig. S1A), which were annotated to 11,561 genes.[23] Using the DepMap database, we screened out 4956 potential dependency genes whose expression or existence might be critical for T-ALL cell line survival or proliferation (Fig. 2C; Fig. S1B). When gene sets in each omics analysis intersected with each other, 29 PPGs were obtained for further study (Fig. 2D); these genes showed a positive correlation between gene expression and chromatin accessibility (Spearman correlation = 0.51, P-value = 0.005; Fig. 2E).
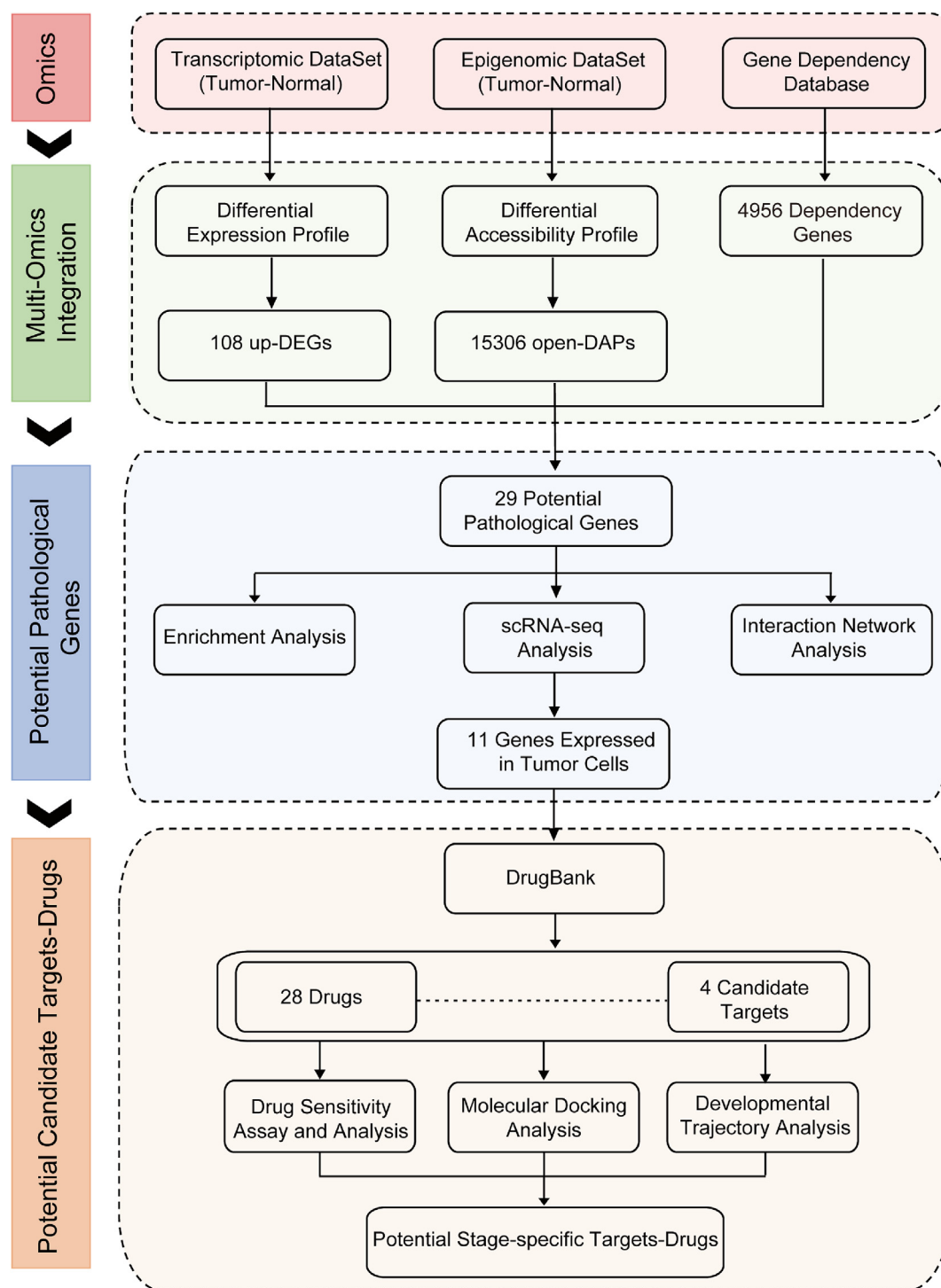
Figure 1 Schematic representation of study workflow for identifying potential candidate stage-specific targets and drugs for T-ALL. DEGs, differentially expressed genes; DAPs, differentially accessible peaks.

Table 1 Summary of three bulk transcriptomic datasets.

Source	Sample type	Number of samples	Reference
GSE26713	Normal/tumor	7 normal and 117 tumor samples	21
GSE48558	Normal/tumor	17 normal and 13 tumor samples	22
Erarslan-Uysal et al	Normal/tumor	3 normal and 19 tumor samples	23
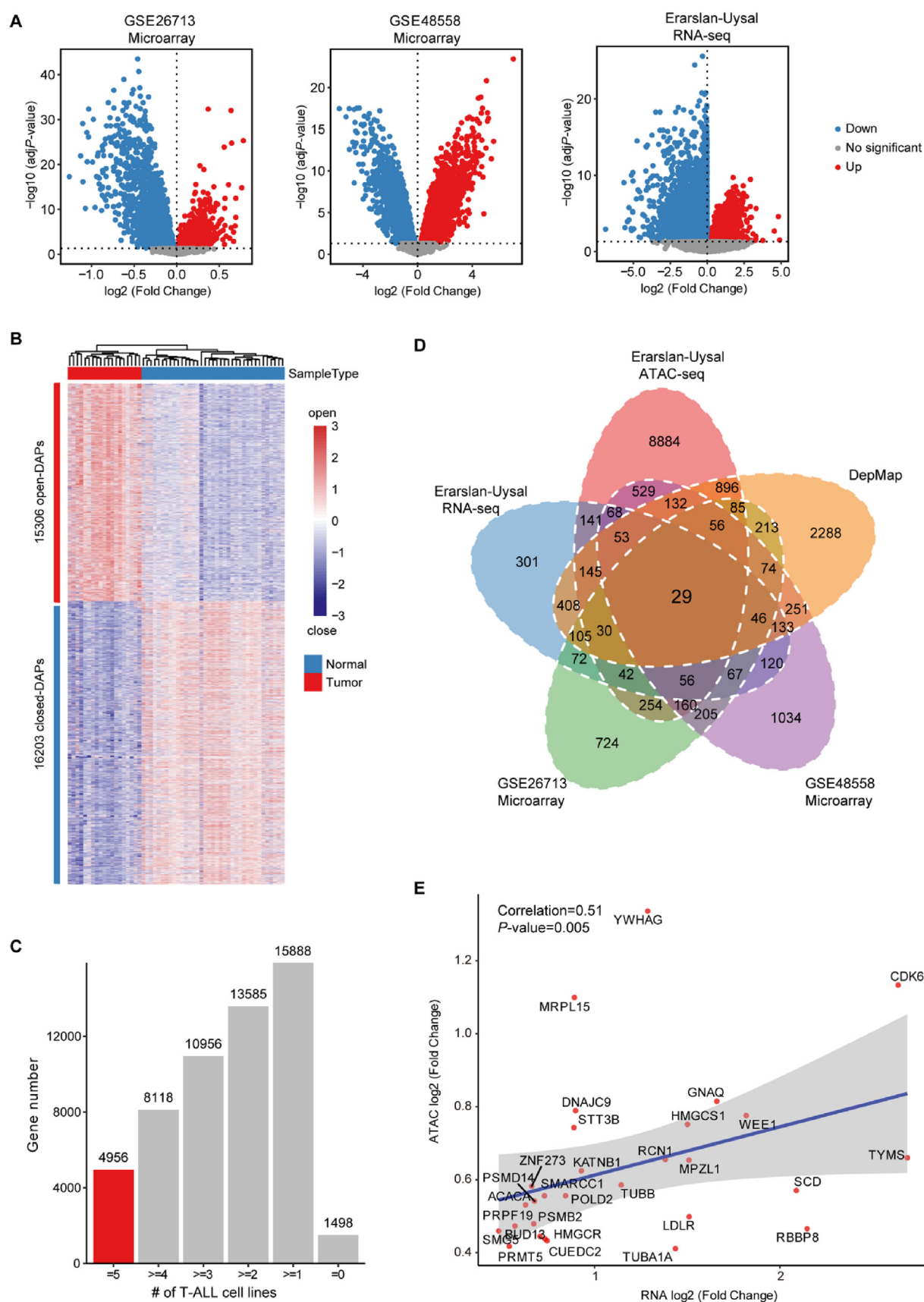
Figure 2 Identification of T-ALL-related PPGs. **(A)** Volcano plots of genes differentially expressed between normal controls and T-ALL samples. Red and blue indicate up-regulated and down-regulated genes, respectively. **(B)** The heatmap showing profiles of

Clinical value of PPGs in T-ALL

To determine the clinical significance of these PPGs, we integrated the expression profiles of three independent cohorts (Fig. S2A). We found that these PPGs had the discriminative ability not only between tumor and normal tissues but also between T-ALL and other hematological diseases (Fig. 3A). Moreover, most PPGs were found to be differentially expressed across T-ALL subtypes dominated by oncogenic TFs (Fig. 3B). ETP-ALL has inferior prognosis[7]; therefore, we next examined the association between PPGs and T-ALL subtypes (ETP, nearETP, and nonETP). Almost two-thirds of the PPGs showed significantly different expression levels between the various subtypes (Fig. 3C; Fig. S2B) and one-third showed significantly different expression levels across different WBC groups (Fig. S2C). Thus, the results indicated that these PPGs might play differing roles in different T-ALL subtypes.

To investigate the association between PPG expression levels and prognosis in T-ALL, we divided the patients from the TARGET cohort into two groups on the basis of the median expression level of each PPG. CDK6 was found to be an unfavorable gene significantly associated with both EFS and OS in T-ALL. KATNB1, ACACA, CUEDC2, and STT3B were found to be unfavorable genes significantly associated with EFS or OS (Fig. 3D). Additionally, pairwise Pearson correlations analysis showed a higher co-expression correlation of PPGs in T-ALL than in normal tissues, further indicating PPG dysfunction in T-ALL (Fig. S2D).

Biological network and functional enrichment analysis

To gain insights into the potential molecular role of PPGs in T-ALL, we performed biological network and functional enrichment analyses. The GGI network contained 49 human genes (nodes) and 533 interactions (edges) and mainly included co-expression (56.23%) and physical interactions (20.55%) (Fig. 4A). We found that several T-ALL onco-functional genes showed the highest interaction with PPGs; for example, HOXA9, which cooperated with activated JAK/STAT signaling to drive T-ALL development,[46] was the highest interaction partner (Fig. 4A). On the basis of the STRING database, the PPI network was constructed with PPGs, yielding 29 nodes, 30 edges, and a PPI enrichment P-value of 8.53e-07 (Fig. S3).

To examine the functional association of PPGs with known T-ALL—associated genes, we measured the shortest path lengths between genes. The mean distance of PPGs from known T-ALL-associated genes was significantly shorter than that between randomly selected genes and known T-ALL-associated genes (P-value = 0; Fig. 4B). These findings suggested that PPGs had a significant functional association with known T-ALL-associated genes.

BP enrichment results showed that PPGs were significantly enriched in the cell cycle, hematopoietic stem cell differentiation, and AMPK signaling pathway, which were closely associated with T-ALL metabolism and tumorigenesis (Fig. 4C). Similarly, KEGG pathway analysis showed that PPGs were enriched in the cell cycle (Fig. 4D). Moreover, tissue enrichment results showed that leukemic cells comprised the most significantly enriched tissue, further indicating the pathological relationship of PPGs with T-ALL (Fig. 4E).

## Screening potential candidate targets and drugs for T-ALL

T-ALL is an aggressive hematologic cancer caused by the malignant transformation of T-cell progenitors[1]; therefore, PPGs highly expressed in malignant T-cells were preferentially considered as potential candidate targets. Therefore, we retrieved single-cell transcriptomic datasets of six patients with primary T-ALL from a study by Thillo et al[25] and found that 11 PPGs were highly expressed in malignant T-cells (Fig. 5A). Of these 11 PPGs, five genes, that is, CDK6, PSMB2, TUBA1A, TUBB, and TYMS, which were mainly involved in the cell cycle, were druggable targets for 30 drugs. These drugs included 17 Food and Drug Administration (FDA)-approved and 13 investigational drugs (Fig. 5B and Table S1). We found these 30 drugs did not have any clinical trials records in T-ALLs from the ClinicalTrails.gov website (https://clinicaltrials.gov/ct2/home), but serval drugs have been trialed for other hematological disorders, such as alvocidib (DB03496) has been tested for AML (e.g., NCT03298984) and chronic lymphocytic leukemia (e.g., NCT00464633), while some drugs have already been trialed for some solid tumors, such as palbociclib (DB0907) have been trialed in breast cancer (e.g., NCT04130152). Excluding PSMB2, the remaining four genes showed significantly higher expression levels in patients with T-ALL than in normal controls from our CHCQMU cohort (Fig. 5C).[24] These four genes also had significantly higher expression levels in T-ALL cell lines than in other cell lines from the CCLE database (Fig. S4A).

To examine the sensitivity of drugs targeting the four potential candidate genes against T-ALL, we further searched the drug-sensitivity database. Ten of the drugs in the NCI-60 database had been tested against two of the T-ALL cell lines (i.e., MOLT4 and CCRF-CEM); these cell lines were sensitive to all the 10 drugs (Fig. 5D). Molecular docking analysis showed that, excluding phenethyl isothiocyanate, the remaining nine drugs showed stable binding affinities with their corresponding targets (Fig. S4B, C). These results indicated that four genes and nine drugs might serve as potential targets and repositioned drugs, respectively, for patients with T-ALL.

Developmental trajectory revealed T-ALL cells arrested at different stages

To precisely identify stage-specific therapeutic targets, we examined the expression patterns of the four candidate genes in malignant T cells. We further classified malignant T

DAPs for normal control and tumor samples. Red and blue represent peaks increasing accessibility (open) and peaks decreasing accessibility (close), respectively. **(C)** The bar plot showing the numbers of potential dependency genes. **(D)** The Venn diagram showing the intersection numbers of gene intersections in each multi-omics dataset. **(E)** Spearman correlation of peak accessibility versus gene expression for PPGs.
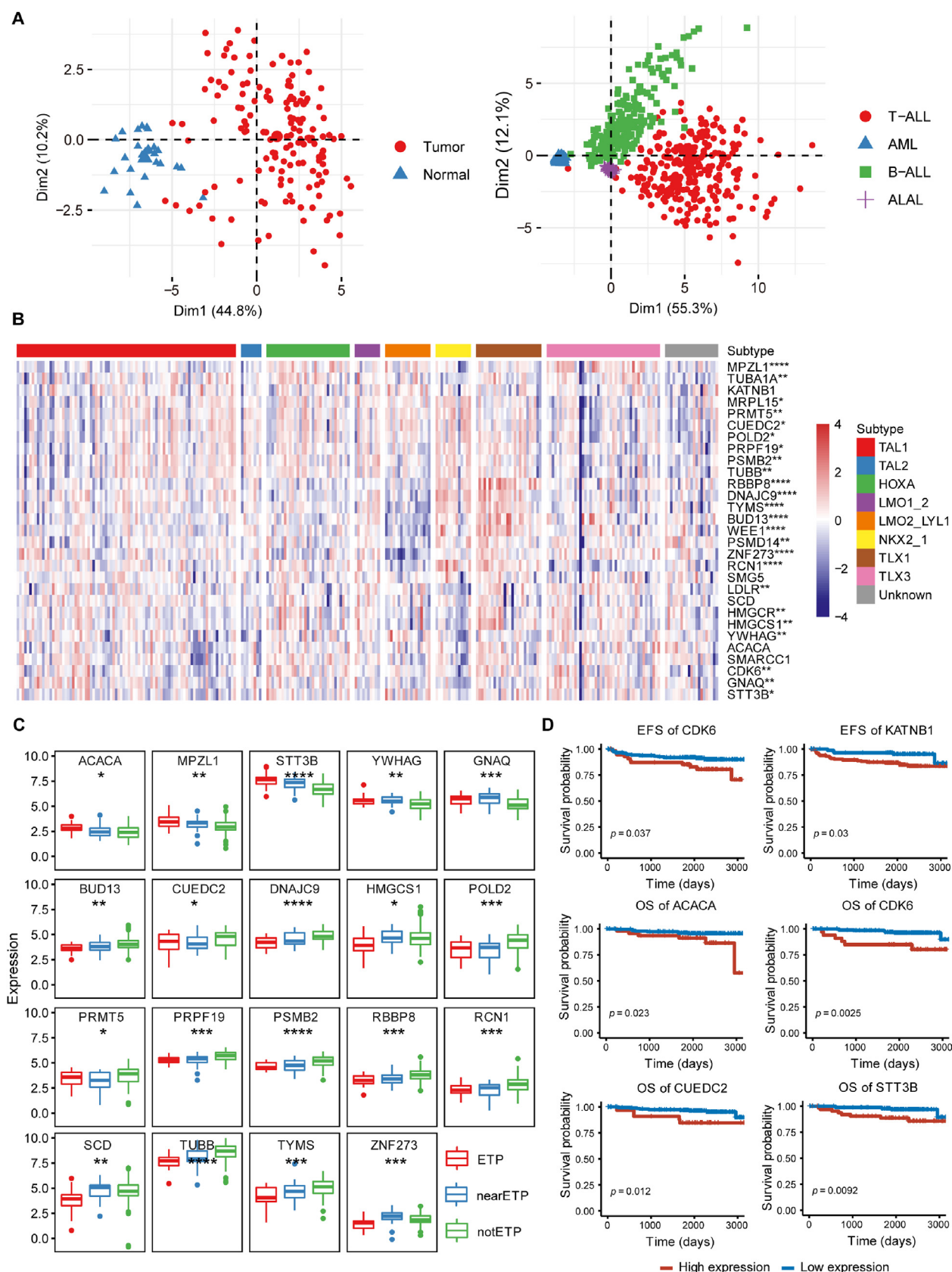
Figure 3   Clinical significance of PPGs. **(A)** The PCA plots showing sample distribution based on PPG expression profiles in different tissue types (left) and leukemias (right). **(B)** The heatmap showing expression profiles of PPGs among TF subtypes. **(C)** The boxplot showing PPG expression across different ETP statuses. **(D)** KM curves of PPG expression in patients with T-ALL from the

cells into six clusters (C1—C6) corresponding to three development stages of T-cell progenitors, that is, the ETP, double-positive (DP), and single-positive (SP) stages (Fig. 6A). The signatures from Liu et al[6] and Zhang et al[47] further confirmed enrichment in the ETP and nonETP signatures (Fig. S5A). The C1—C3 clusters were considered ETP-ALL cells, which expressed higher levels of hematopoietic stem markers like CD34, while the C4—C6 clusters expressed higher levels of mature T-cell markers like CD1E and CD3D (Fig. 6B; Fig. S5B). C4 cluster was considered as the DP stage, wherein CD3D, CD4, and CD8 were expressed, while C5 and C6 clusters were blocked at the SP stage, wherein only CD8 was highly expressed (Fig. 6B).

To determine lineage differentiation among these diverse malignant T-cells, we performed developmental trajectory analysis, which showed that C1—C6 clusters corresponded to the development process of normal T-cell progenitors, namely, the ETP to DP to SP stages, which further validated our stage classification (Fig. 6C; Fig. S5C).

Potential stage-specific targets and repositioned drugs for T-ALL

To gain insights into the expression patterns of the four druggable targets in normal developmental thymocytes and T-ALL, we analyzed the scRNA-seq data of human thymus[26] and T-ALL samples.[25] The expression patterns of the four potential targets in T-ALL were dysregulated in comparison with those in normal developmental thymocytes (Fig. 7A, B). Specifically, TUBA1A was highly expressed in leukemia cells blocked at immature stages, that is, mainly in ETP-ALL cells, while TYMS and TUBB were mainly expressed in malignant T cells arrested at the DP or SP stage, that is, cortical or mature T-ALL cells. CDK6 showed a U-shaped expression pattern along the course of malignant T cell development (Fig. 7B; Fig. S6A).

To further validate the role of the four potential druggable targets and their corresponding drugs, we performed the cell proliferation assay for seven T-ALL cell lines, that is, PEER, CCRF-CEM, P12, MOLT3, MOLT4, CUTTL1, and JURKAT. Based on cell surface markers and findings of previous studies,[5,48,49] we classified these T-ALL cell lines into distinct developmental stages (Fig. S6B, C). Based on the T cell receptor (TCR) activation status, PEER and CCRF-CEM were classified into TCR-inactive cell lines, while the remaining cell lines were classified into TCR-active cell lines (Fig. S6D). TUBA1A and TYMS exhibited more obvious stage-specific expression trends and their functions in T-ALL were not known (Fig. 7B); therefore, we focused on these two genes and their corresponding FDA-approved inhibitors (mebendazole and gemcitabine, respectively), to examine their potential stage-specific roles in T-ALL. For mebendazole, PEER and CCRF-CEM, that is, TCR-inactive cell lines blocked at immature stages, showed higher drug sensitivities than TCR-active T-ALL cell lines (Wilcoxon test, P value = 0.048) *in vitro* (Fig. 7C, D). In contrast,

gemcitabine exerted greater inhibitory effects on all the TCR-active cell lines than on the TCR-inactive cell line CCRF-CEM (Fig. 7C, D). The T-ALL stages in which these two drugs had greater inhibitory effects were consistent with the T-ALL stages in which their targets were highly expressed. Taken together, the results indicated that these potential targets and drugs might exert stage-specific antileukemic effects in T-ALL.

Discussion

The increasing characterization of T-ALL has helped identify several molecular targets[8–12]; however, these findings have yet to be translated into more effective targeted treatments because of T-ALL heterogeneity. In the current study, we integrated multi-omics data to identify 29 PPGs. PCA showed that PPGs exhibited tissue-specific expression profiles, indicating their potential as diagnostic signatures. scRNA-seq analysis showed that, among the PPGs, CDK6, TUBA1A, TUBB, and TYMS, which are known druggable genes, were dysregulated and exhibited stage-specific expression levels in malignant T cells. In addition, mebendazole and gemcitabine (TUBA1A and TYMS inhibitors, respectively) exerted stage-specific inhibitory effects on the T-ALL cell lines.

Although genomic analysis has been used to examine the underlying pathogenesis of T-ALL, epigenomic and transcriptomic analyses have been widely applied to investigate thymocyte development and characterize tumor biology.[6,23,25,50] Emerging single-cell technology has also been used to examine T-ALL molecular pathogenesis.[25,50] Using scRNA-seq analysis, Thillo et al revealed that TCF7-SPI1 T-ALL was vulnerable to pharmacological targeting of the TCF/β-catenin interaction.[25] Bie et al reported that targeted single-cell sequencing could help determine the order of mutation acquisition in T-ALL.[50] T-ALL is a complex disease and a single-omics analysis would not be sufficiently powerful for its analysis[51]; many recent studies have indicated that multi-omics integration analysis can help obtain more scientific knowledge. Therefore, in this study, we integrated mRNA expression, chromatin accessibility, and gene-dependency database analyses and identified 29 PPGs involved in T-ALL pathogenesis. Furthermore, GO and KEGG analyses showed that these PPGs were significantly enriched in the cell cycle. Loss of cell cycle control plays a prominent role in T-ALL pathogenesis.[6] Previous research showed that cell cycle dysfunction was caused by recurrent cytogenetic and molecular alterations, which was a common feature in all T-ALL molecular subtypes.[52]

T-ALL is a heterogeneous malignant tumor that arises during the differentiation stages of intra-thymic T-cell progenitors[1]; therefore, it is essential to develop precisely individualized treatments. We focused on leukemia cells to identify candidate druggable targets at the single-cell level. Four known druggable genes, that is, CDK6, TUBA1A, TUBB, and TYMS, showed high expression levels in malignant T cells (Fig. 5A—C). Compared with the expression trends in normal T cell development, these four genes
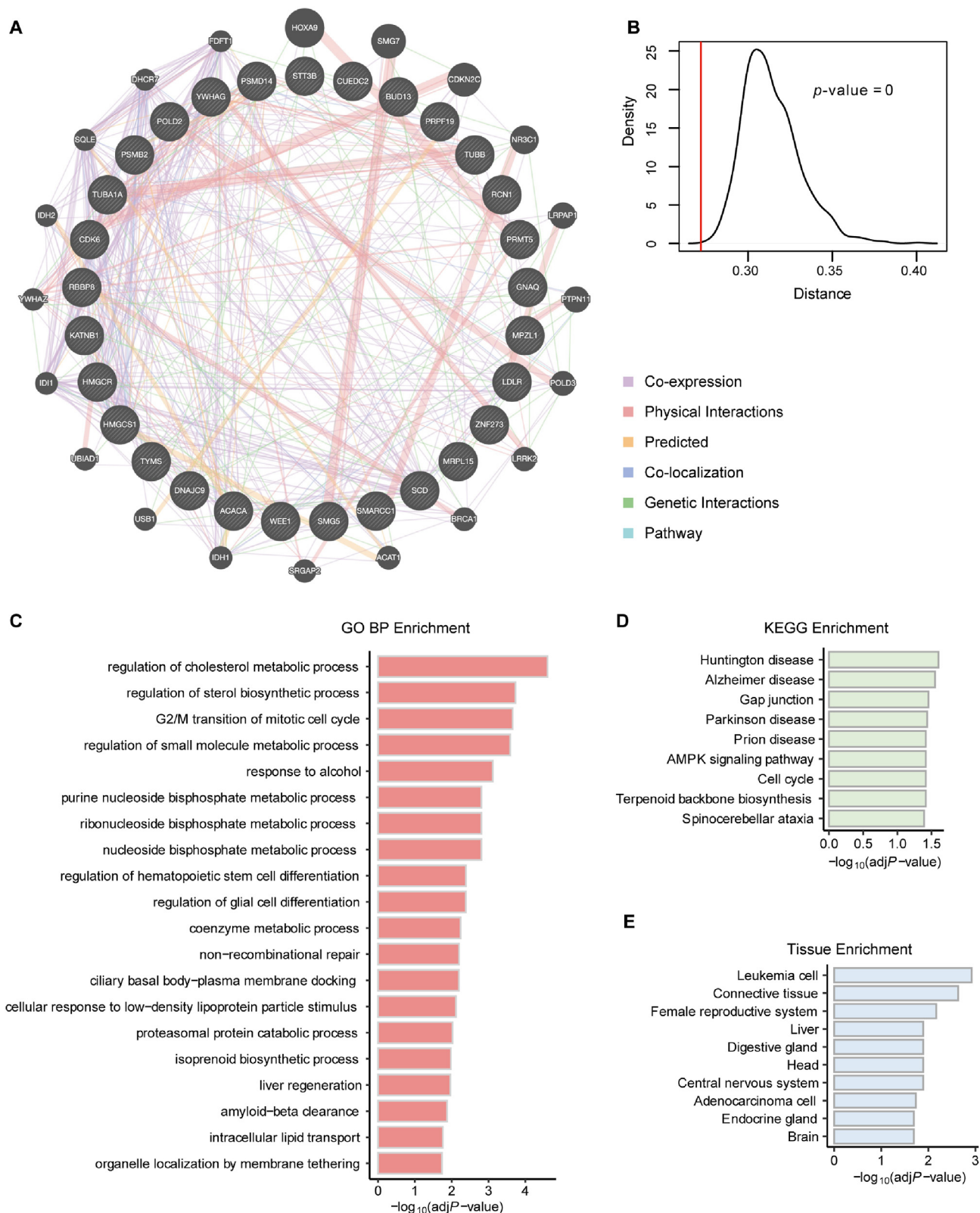
Figure 4 Biological network and functional enrichment analysis of PPGs. **(A)** GGI network clusters of PPGs. **(B)** Distributions of the mean shortest path lengths of randomly selected genes. Red lines mark the actual mean shortest path lengths between 29 PPGs and known T-ALL-associated disease genes from the GAD database. Black lines represent the distributions of the mean shortest path lengths between randomly selected genes and known T-ALL-associated genes. **(C–E)** Visualization of enriched terms in (C) BP terms (D) KEGG pathways, and (E) tissues. An adjusted P-value <0.05 was considered significant.
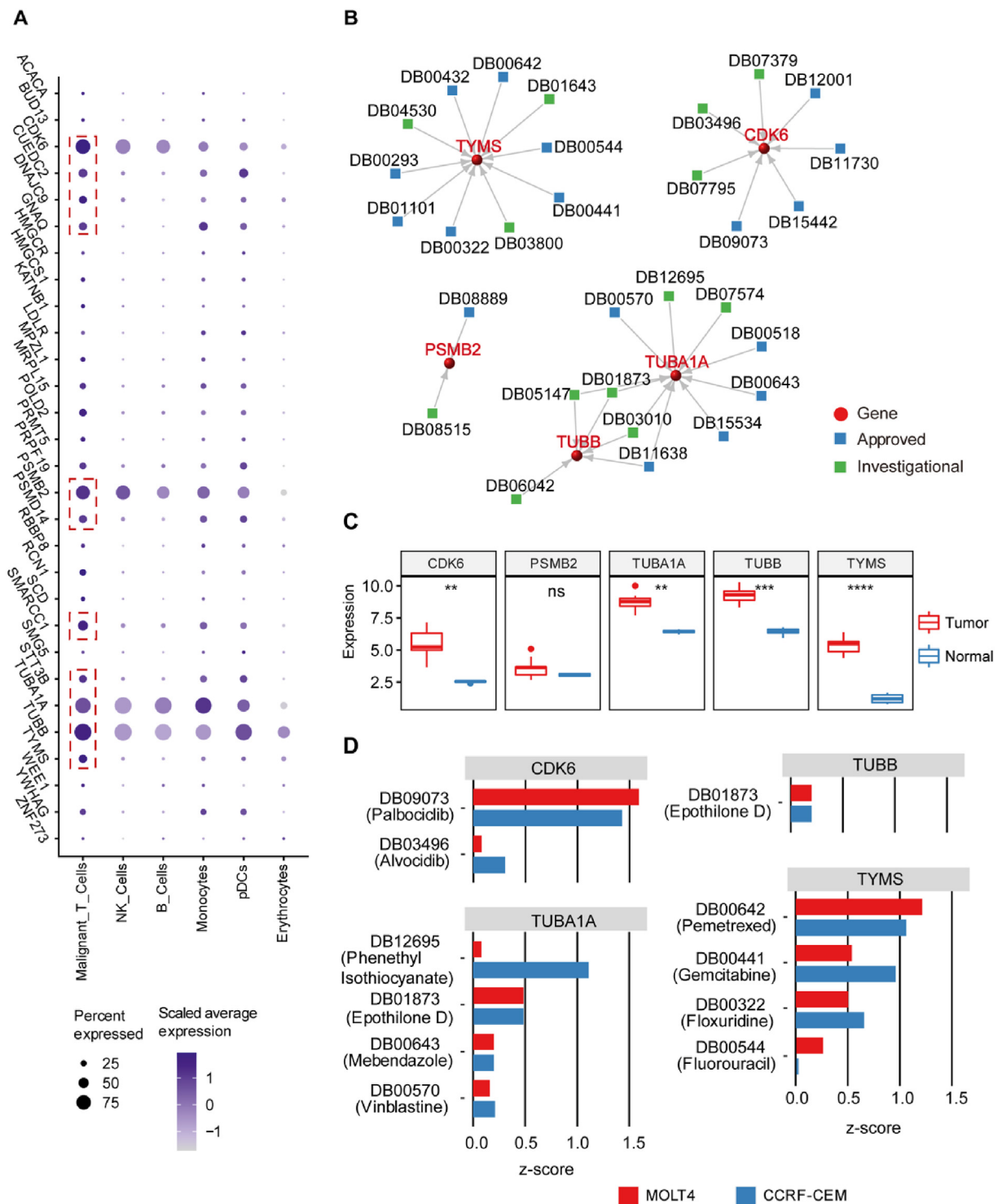
Figure 5 Identification of potential candidate targets and drugs for T-ALL. **(A)** The dot plot showing the scaled average expression of PPGs for different cell types. Dot size represents the proportion of cells expressing a specific gene in that cell type. The dot color represents the scaled average expression. **(B)** Gene-drug network constructed from the DrugBank database by using Cytoscape. The red dot represents a gene, the blue square represents an approved drug, and the green square represents an investigational drug. **(C)** The boxplot displaying expression levels of five candidates in tumor and normal samples from the CHCQMU cohort. **(D)** The bar plot showing the z-score from the NCI-60 database. A z-score >0 indicates the sensitivity of T-ALL cell lines for candidate drugs. *adj$P < 0.05$, **adj$P < 0.005$, ***adj$P < 0.0005$, ****adj$P < 0.00005$; ns, no significant differences.
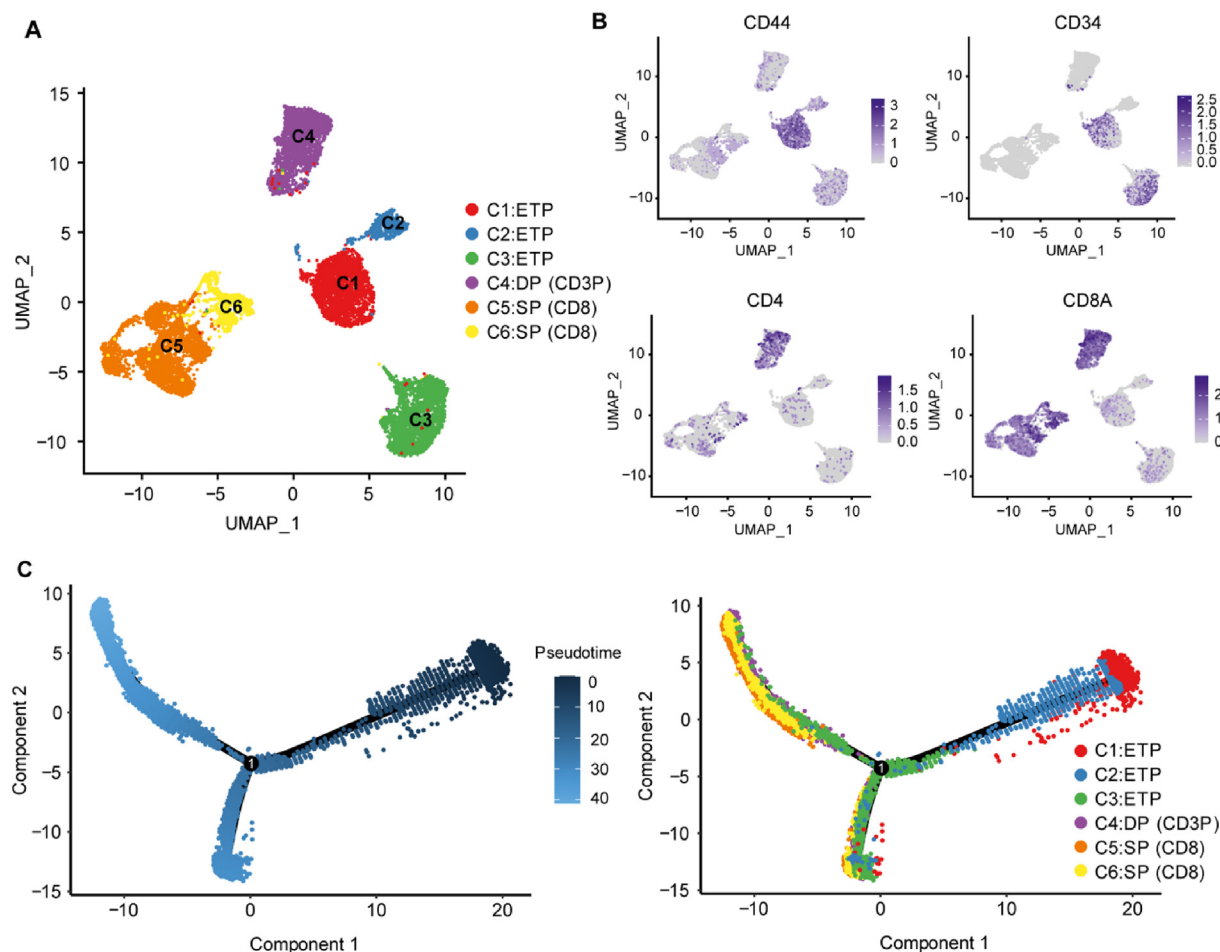
Figure 6 Identification of malignant T-cell stage, based on scRNA-seq data. **(A)** UMAP projection of malignant T-cells in T-ALL. Each dot represents a cell. **(B)** UMAP plots of marker genes expressed in malignant T-cells. Colored bars indicate expression levels. **(C)** Developmental trajectory of malignant T-cells inferred by Monocle and visualized on the UMAP based on pseudotime scores (left) and stages (right). The pseudotime scores from dark blue to light blue indicate the stages from early to the terminal.

showed dysregulated and stage-specific expression trends along the course of malignant T cell development ([Fig. 7]A, B). TUBA1A was expressed during the early development stage of malignant T-cells, while TYMS was specifically expressed during the later development stage of leukemia cells. TUBA1A and TYMS inhibitors (mebendazole and gemcitabine, respectively) also exerted stage-specific inhibitory effects on T-ALL cell lines.

TUBA1A encodes an alpha tubulin protein, which is part of the microtubule protein structure.[53] Microtubules are essential for many cellular processes, including cell division, cell motility, cell shape maintenance, and intracellular trafficking.[54] Microtubule dynamics are disrupted during cancer cell division and have been implicated in chromosomal instability and drug resistance.[55] Previous studies reported that TUBA1A is a prognostic marker highly expressed in several cancers.[56,57] Additionally, TUBA1A acetylation is vital for cancer cell adhesion and migration.[58] We found that TUBA1A showed higher expression in leukemia cells arrested at the immature stage ([Fig. 7]B). Consistent with these findings, mebendazole, a TUBA1A inhibitor, also exerted greater inhibitory effects on TCR-inactive cell lines than on TCR-active cell lines. Mebendazole has been

approved by the FDA for treating human helminthic infections and has a long track record of safe human use[59]; studies have suggested its use as a repositioned drug for medulloblastoma[60] and glioblastoma.[61]

TYMS, a thymidylate synthetase, is involved in DNA biosynthesis, which is essential for cell survival.[62] TYMS is the target gene of E2F1, a potent oncogene involved in cell cycle progression, apoptosis, and the DNA-damage response.[63] Increased TYMS expression leads to an increase in cancer cell aggressiveness and metastasis.[64,65] Increasing studies have reported that TYMS is a critical therapeutic target for several cancer drugs.[66,67] We found TYMS was highly expressed in malignant T cells blocked at a relatively late stage ([Fig. 7]B) and that its inhibitor gemcitabine also had higher drug toxicity in all TCR-active cell lines than in the TCR-inactive cell line CCRF-CEM ([Fig. 7]C). Gemcitabine has been approved by the FDA for treating cancers such as testicular, breast, ovarian, and non-small cell lung cancers.[68] Our results indicated that mebendazole and gemcitabine had the potential as stage-specific repositioned drugs for T-ALL.

CDK6, a serine/threonine protein kinase, controls the cell cycle and differentiation,[69] which is required for
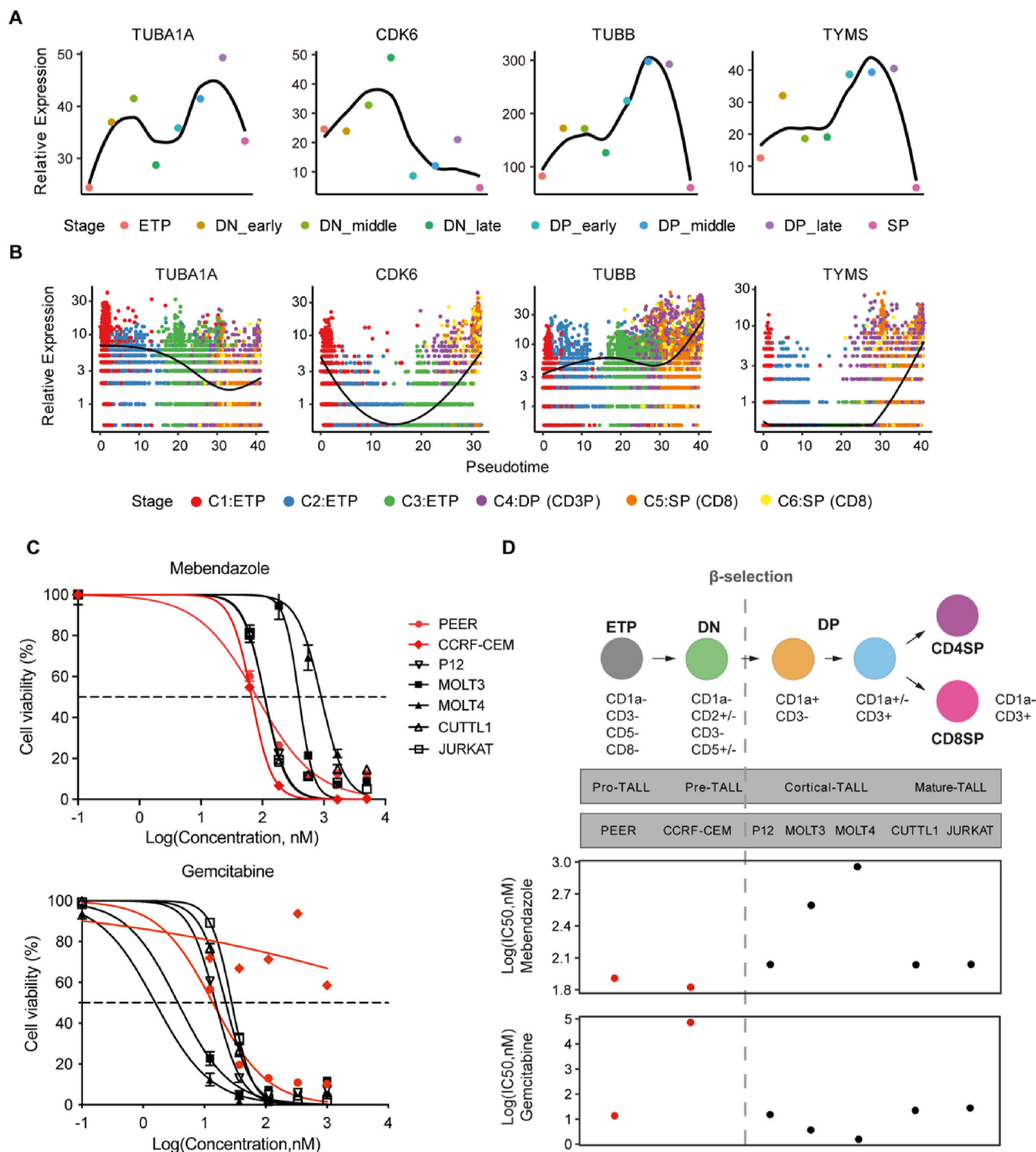
Figure 7 Potential stage-specific targets and repositioned drugs for T-ALL. **(A, B)** The kinetics plot showing dynamic changes in candidate target expression along with normal T cell (A) and malignant T cell (B) development. **(C)** Cell viability curve for T-ALL cell lines treated with increasing mebendazole (upper) and gemcitabine (lower) concentrations. **(D)** Upper, schematic representation of human thymocyte development from ETP to DN, DP, and SP (CD4SP, CD8SP) stages. Middle, T-ALL cell lines assigned to different T-ALL differentiation stages. Lower, half-maximal inhibitory concentration (IC$_{50}$) value after logarithmic transformation of mebendazole and gemcitabine in T-ALL cell lines. Red and black represent TCR-inactive and TCR-active cell lines, respectively.

thymocyte development.[70] There is increasing interest in CDK6 as a candidate target for T-ALL.[14,71,72] In our study, the highest sensitivity to the CDK6 inhibitor palbociclib, a candidate drug, was noted in MOLT4 and CCRF-CEM cells

(Fig. 5D). Recently, Ishio et al[14] also showed that palbociclib can inhibit T-ALL proliferation and survival in adults. TUBB encodes a β-tubulin protein and acts as a microtubule structural component[73]; it mediates the cell cycle,

proliferation, metastasis, and invasion in cutaneous melanoma.[74] The findings obtained using our multi-omics approach might provide a comprehensive resource for identifying potential stage-specific druggable targets and are promising for achieving more precise therapeutic strategies for T-ALL.

Conclusion

Our findings suggested that the candidate druggable targets CDK6, TUBA1A, TUBB, and TYMS showed dysregulated and stage-specific expression in malignant T cells and may serve as stage-specific targets for T-ALL patients. Mebendazole and gemcitabine exerted stage-specific inhibitory effects on the T-ALL cell lines, which indicate their stage-specific antileukemic role in T-ALL and are now being further investigated in preclinical trials in our laboratory. Taken together, our results will provide insights into the use of multi-omics approaches for developing potential targeted therapies for different T-ALL subsets.

Author contributions

LZ and YS guided and supervised this study. ZJY designed this study. ZJY participated in data collection, data processing, program implementation, and manuscript writing. JX contributed to molecular docking analysis and manuscript writing. YZC, YHZ, XJW, and NTF proofread the manuscript. All authors provided critical advice regarding the final manuscript.

Conflict of interests

The authors delcare that there is no competing interest.

Funding

Data availability

The datasets downloaded and/or analyzed during the current study have been obtained from publicly available datasets. These data can be found here: www.ncbi.nlm.nih.gov/geo, Erarslan-Uysal et al,[23] https://ocg.cancer.gov/programs/target/data-matrix, https://zenodo.org/record/4756105#.YMbypC0RqqB, and https://developmentcellatlas.ncl.ac.uk. The relevant scripts are available at https://github.com/YZJenny/TALL-GD.

Acknowledgements

Appendix A. Supplementary data

Supplementary data to this article can be found online at https://doi.org/10.1016/j.gendis.2023.03.022.

References

1. Pui CH, Robison LL, Look AT. Acute lymphoblastic leukaemia. *Lancet*. 2008;371(9617):1030−1043.
2. Tang J, Yu J, Cai J, et al. Prognostic factors for CNS control in children with acute lymphoblastic leukemia treated without cranial irradiation. *Blood*. 2021;138(4):331−343.
3. Goldstone AH, Richards SM, Lazarus HM, et al. In adults with standard-risk acute lymphoblastic leukemia, the greatest benefit is achieved from a matched sibling allogeneic transplantation in first complete remission, and an autologous transplantation is less effective than conventional consolidation/maintenance chemotherapy in all patients: final results of the International ALL Trial (MRC UKALL XII/ECOG E2993). *Blood*. 2008;111(4):1827−1833.
4. Kozlowski P, Åström M, Ahlberg L, et al. High relapse rate of T cell acute lymphoblastic leukemia in adults treated with Hyper-CVAD chemotherapy in Sweden. *Eur J Haematol*. 2014;92(5):377−381.
5. Bene MC, Castoldi G, Knapp W, et al. Proposals for the immunological classification of acute leukemias. European group for the immunological characterization of leukemias (EGIL). *Leukemia*. 1995;9(10):1783−1786.
6. Liu Y, Easton J, Shao Y, et al. The genomic landscape of pediatric and young adult T-lineage acute lymphoblastic leukemia. *Nat Genet*. 2017;49(8):1211−1218.
7. Coustan-Smith E, Mullighan CG, Onciu M, et al. Early T-cell precursor leukaemia: a subtype of very high-risk acute lymphoblastic leukaemia. *Lancet Oncol*. 2009;10(2):147−156.
8. Weng AP, Ferrando AA, Lee W, et al. Activating mutations of NOTCH1 in human T cell acute lymphoblastic leukemia. *Science*. 2004;306(5694):269−271.
9. Graux C, Cools J, Melotte C, et al. Fusion of NUP214 to ABL1 on amplified episomes in T-cell acute lymphoblastic leukemia. *Nat Genet*. 2004;36(10):1084−1089.
10. Flex E, Petrangeli V, Stella L, et al. Somatically acquired JAK1 mutations in adult acute lymphoblastic leukemia. *J Exp Med*. 2008;205(4):751−758.
11. Shochat C, Tal N, Bandapalli OR, et al. Gain-of-function mutations in interleukin-7 receptor-alpha (IL7R) in childhood acute lymphoblastic leukemias. *J Exp Med*. 2011;208(5):901−908.
12. Zenatti PP, Ribeiro D, Li W, et al. Oncogenic IL7R gain-of-function mutations in childhood T-cell acute lymphoblastic leukemia. *Nat Genet*. 2011;43(10):932−939.
13. Knoechel B, Roderick JE, Williamson KE, et al. An epigenetic mechanism of resistance to targeted therapy in T cell acute lymphoblastic leukemia. *Nat Genet*. 2014;46(4):364−370.
14. Ishio T, Kumar S, Shimono J, et al. Genome-wide CRISPR screen identifies CDK6 as a therapeutic target in adult T-cell leukemia/lymphoma. *Blood*. 2022;139(10):1541−1556.
15. Rodriguez S, Abundis C, Boccalatte F, et al. Therapeutic targeting of the E3 ubiquitin ligase SKP$_2$ in T-ALL. *Leukemia*. 2020;34(5):1241−1252.
16. Subramaniam PS, Whye DW, Efimenko E, et al. Targeting nonclassical oncogenes for therapy in T-ALL. *Cancer Cell*. 2012;21(4):459−472.
17. Hasin Y, Seldin M, Lusis A. Multi-omics approaches to disease. *Genome Biol*. 2017;18(1):83.

18. Wang Y, Yang Y, Chen S, et al. DeepDRK: a deep learning framework for drug repurposing through kernel-based multi-omics integration. *Briefings Bioinf*. 2021;22(5):bbab048.

19. Aydin B, Beklen H, Arga KY, et al. Epigenomic and transcriptomic landscaping unraveled candidate repositioned therapeutics for non-functioning pituitary neuroendocrine tumors. *J Endocrinol Invest*. 2023;46(4):727–747.

20. Tang F, Barbacioru C, Wang Y, et al. mRNA-Seq whole-transcriptome analysis of a single cell. *Nat Methods*. 2009;6(5):377–382.

21. Homminga I, Pieters R, Langerak AW, et al. Integrated transcript and genome analyses reveal *NKX2-1* and *MEF2C* as potential oncogenes in T cell acute lymphoblastic leukemia. *Cancer Cell*. 2011;19(4):484–497.

22. Cramer-Morales K, Nieborowska-Skorska M, Scheibner K, et al. Personalized synthetic lethality induced by targeting RAD52 in leukemias identified by gene mutation and expression profile. *Blood*. 2013;122(7):1293–1304.

23. Erarslan-Uysal B, Kunz JB, Rausch T, et al. Chromatin accessibility landscape of pediatric T-lymphoblastic leukemia and human T-cell precursors. *EMBO Mol Med*. 2020;12(9), e12104.

24. Shu Y, Wang Y, Lv WQ, et al. ARRB1-promoted NOTCH1 degradation is suppressed by OncomiR miR-223 in T-cell acute lymphoblastic leukemia. *Cancer Res*. 2020;80(5):988–998.

25. Van Thillo Q, De Bie J, Seneviratne JA, et al. Oncogenic cooperation between TCF7-SPI$_1$ and NRAS(G12D) requires β-catenin activity to drive T-cell acute lymphoblastic leukemia. *Nat Commun*. 2021;12(1):4164.

26. Park JE, Botting RA, Domínguez Conde C, et al. A cell atlas of human thymic development defines T cell repertoire formation. *Science*. 2020;367(6480), eaay3224.

27. Ritchie ME, Phipson B, Wu D, et al. Limma powers differential expression analyses for RNA-sequencing and microarray studies. *Nucleic Acids Res*. 2015;43(7):e47.

28. Tsherniak A, Vazquez F, Montgomery PG, et al. Defining a cancer dependency map. *Cell*. 2017;170(3):564–576.e16.

29. Szklarczyk D, Gable AL, Lyon D, et al. STRING v11: protein-protein association networks with increased coverage, supporting functional discovery in genome-wide experimental datasets. *Nucleic Acids Res*. 2019;47(D1):D607–D613.

30. Warde-Farley D, Donaldson SL, Comes O, et al. The GeneMANIA prediction server: biological network integration for gene prioritization and predicting gene function. *Nucleic Acids Res*. 2010;38(Web Server issue):W214–W220.

31. Yu G, Wang LG, Han Y, et al. clusterProfiler: an R package for comparing biological themes among gene clusters. *OMICS*. 2012;16(5):284–287.

32. Ni Q, Su X, Chen J, et al. Prediction of metabolic gene biomarkers for neurodegenerative disease by an integrated network-based approach. *BioMed Res Int*. 2015;2015, 432012.

33. Becker KG, Barnes KC, Bright TJ, et al. The genetic association database. *Nat Genet*. 2004;36(5):431–432.

34. Alexeyenko A, Schmitt T, Tjärnberg A, et al. Comparative interactomics with funcoup 2.0. *Nucleic Acids Res*. 2012;40(Database issue):D821–D828.

35. Law V, Knox C, Djoumbou Y, et al. DrugBank 4.0: shedding new light on drug metabolism. *Nucleic Acids Res*. 2014;42(Database issue):D1091–D1097.

36. Ghandi M, Huang FW, Jané-Valbuena J, et al. Next-generation characterization of the cancer cell line encyclopedia. *Nature*. 2019;569(7757):503–508.

37. Reinhold WC, Sunshine M, Liu H, et al. CellMiner: a web-based suite of genomic and pharmacologic tools to explore transcript and drug patterns in the NCI-60 cell line set. *Cancer Res*. 2012;72(14):3499–3511.

38. Burley SK, Berman HM, Christie C, et al. RCSB Protein Data Bank: sustaining a living digital data resource that enables breakthroughs in scientific research and biomedical education. *Protein Sci*. 2018;27(1):316–330.

39. Biovia DS. *Discovery Studio Modeling Environment, Release 2017*. San Diego: DassaultSystèmes; 2016.

40. Sterling T, Irwin JJ. ZINC 15: ligand discovery for everyone. *J Chem Inf Model*. 2015;55(11):2324–2337.

41. Kim S, Thiessen PA, Bolton EE, et al. PubChem substance and compound databases. *Nucleic Acids Res*. 2016;44(D1):D1202–D1213.

42. Trott O, Olson AJ. AutoDock Vina: improving the speed and accuracy of docking with a new scoring function, efficient optimization, and multithreading. *J Comput Chem*. 2010;31(2):455–461.

43. Yao H, Xie S, Ma X, et al. Identification of a potent oridonin analogue for treatment of triple-negative breast cancer. *J Med Chem*. 2020;63(15):8157–8178.

44. Butler A, Hoffman P, Smibert P, et al. Integrating single-cell transcriptomic data across different conditions, technologies, and species. *Nat Biotechnol*. 2018;36(5):411–420.

45. Bray NL, Pimentel H, Melsted P, et al. Near-optimal probabilistic RNA-seq quantification. *Nat Biotechnol*. 2016;34(5):525–527.

46. de Bock CE, Demeyer S, Degryse S, et al. HOXA9 cooperates with activated JAK/STAT signaling to drive leukemia development. *Cancer Discov*. 2018;8(5):616–631.

47. Zhang J, Ding L, Holmfeldt L, et al. The genetic basis of early T-cell precursor acute lymphoblastic leukaemia. *Nature*. 2012;481(7380):157–163.

48. Kraszewska MD, Dawidowska M, Szczepański T, et al. T-cell acute lymphoblastic leukaemia: recent molecular biology findings. *Br J Haematol*. 2012;156(3):303–315.

49. Greenberg JM, Gonzalez-Sarmiento R, Arthur DC, et al. Immunophenotypic and cytogenetic analysis of Molt-3 and Molt-4:human T-lymphoid cell lines with rearrangement of chromosome 7. *Blood*. 1988;72(5):1755–1760.

50. De Bie J, Demeyer S, Alberti-Servera L, et al. Single-cell sequencing reveals the origin and the order of mutation acquisition in T-cell acute lymphoblastic leukemia. *Leukemia*. 2018;32(6):1358–1369.

51. Karczewski KJ, Snyder MP. Integrative omics for health and disease. *Nat Rev Genet*. 2018;19(5):299–310.

52. Aifantis I, Raetz E, Buonamici S. Molecular pathogenesis of T-cell leukaemia and lymphoma. *Nat Rev Immunol*. 2008;8(5):380–390.

53. Hammond JW, Cai D, Verhey KJ. Tubulin modifications and their cellular functions. *Curr Opin Cell Biol*. 2008;20(1):71–76.

54. Mandelkow E, Mandelkow EM. Microtubules and microtubule-associated proteins. *Curr Opin Cell Biol*. 1995;7(1):72–81.

55. Duijf PHG, Schultz N, Benezra R. Cancer cells preferentially lose small chromosomes. *Int J Cancer*. 2013;132(10):2316–2326.

56. Nami B, Wang Z. Genetics and expression profile of the tubulin gene superfamily in breast cancer subtypes and its relation to taxane resistance. *Cancers*. 2018;10(8):274.

57. Wang D, Jiao Z, Ji Y, et al. Elevated TUBA1A might indicate the clinical outcomes of patients with gastric cancer, being associated with the infiltration of macrophages in the tumor immune microenvironment. *J Gastrointestin Liver Dis*. 2020;29(4):509–522.

58. Boggs AE, Vitolo MI, Whipple RA, et al. α-Tubulin acetylation elevated in metastatic and basal-like breast cancer cells promotes microtentacle formation, adhesion, and invasive migration. *Cancer Res*. 2015;75(1):203–215.

59. Wolfe MS, Wershing JM. Mebendazole. Treatment of trichuriasis and ascariasis in Bahamian children. *JAMA*. 1974;230(10):1408–1411.

60. Bai RY, Staedtke V, Rudin CM, et al. Effective treatment of diverse medulloblastoma models with mebendazole and its impact on tumor angiogenesis. *Neuro Oncol*. 2015;17(4):545–554.

61. Bai RY, Staedtke V, Aprhys CM, et al. Antiparasitic mebendazole shows survival benefit in 2 preclinical models of glioblastoma multiforme. *Neuro Oncol*. 2011;13(9):974–982.

62. Ntavatzikos A, Spathis A, Patapis P, et al. TYMS/KRAS/BRAF molecular profiling predicts survival following adjuvant chemotherapy in colorectal cancer. *World J Gastrointest Oncol*. 2019;11(7):551–566.

63. Denechaud PD, Fajas L, Giralt A. E2F1, a novel regulator of metabolism. *Front Endocrinol(Lausanne)*. 2017;8:311.

64. Zhang F, Ye J, Guo W, et al. TYMS-TM4SF$_4$ axis promotes the progression of colorectal cancer by EMT and upregulating stem cell marker. *Am J Cancer Res*. 2022;12(3):1009–1026.

65. Lu Y, Zhuo C, Cui B, et al. TYMS serves as a prognostic indicator to predict the lymph node metastasis in Chinese patients with colorectal cancer. *Clin Biochem*. 2013;46(15):1478–1483.

66. Taddia L, D'Arca D, Ferrari S, et al. Inside the biochemical pathways of thymidylate synthase perturbed by anticancer drugs: novel strategies to overcome cancer chemoresistance. *Drug Resist Updat*. 2015;23:20–54.

67. Fu F, Zhang Y, Gao Z, et al. Development and validation of a five-gene model to predict postoperative brain metastasis in operable lung adenocarcinoma. *Int J Cancer*. 2020;147(2):584–592.

68. Plunkett W, Huang P, Gandhi V. Preclinical characteristics of gemcitabine. *Anti Cancer Drugs*. 1995;6(Suppl 6):7–13.

69. Malumbres M, Barbacid M. Mammalian cyclin-dependent kinases. *Trends Biochem Sci*. 2005;30(11):630–641.

70. Hu MG, Deshpande A, Schlichting N, et al. CDK6 kinase activity is required for thymocyte development. *Blood*. 2011;117(23): 6120–6131.

71. Bride KL, Hu H, Tikhonova A, et al. Rational drug combinations with CDK4/6 inhibitors in acute lymphoblastic leukemia. *Haematologica*. 2022;107(8):1746–1757.

72. Jena N, Sheng J, Hu JK, et al. CDK6-mediated repression of CD25 is required for induction and maintenance of Notch1-induced T-cell acute lymphoblastic leukemia. *Leukemia*. 2016; 30(5):1033–1043.

73. Mesquita B, Veiga I, Pereira D, et al. No significant role for beta tubulin mutations and mismatch repair defects in ovarian cancer resistance to paclitaxel/cisplatin. *BMC Cancer*. 2005;5: 101.

74. Liu Y, Ma S, Ma Q, et al. Silencing LINC00665 inhibits cutaneous melanoma *in vitro* progression and induces apoptosis via the miR-339-3p/TUBB. *J Clin Lab Anal*. 2022; 36(9), e24630.